





Research Article

Trajectory Tracking of Swing-Arm Type Omnidirectional Mobile Robot

Qifan Ran ¹, Shengzhuo Yao ^{1,2}, Xinbo Chen ³, and Guijun Bi ⁴

¹School of Mechanical-electronic and Automobile Engineering, Beijing University of Civil Engineering and Architecture, Beijing 100044, China

²Beijing Engineering Research Center of Monitoring for Construction Safety, Beijing 100044, China

³China North Vehicle Research Institute, Beijing 100072, China

⁴Singapore Institute of Manufacturing Technology (SIMTech), A, Star, 73 Nanyang Drive, 637662, Singapore

Correspondence should be addressed to Shengzhuo Yao; yaoshengzhuo@bucea.edu.cn

Received 25 July 2022; Accepted 10 October 2022; Published 25 October 2022

Academic Editor: Ha Quang Thinh Ngo

Copyright © 2022 QiFan Ran et al. This is an open access article distributed under the Creative Commons Attribution License, which permits unrestricted use, distribution, and reproduction in any medium, provided the original work is properly cited.

In order to enhance the omnidirectional maneuverability of outdoor wheeled mobile robots, a mobile robot driven by a common wheel is proposed, which realizes four-wheel steering (4WS), oblique motion mode, and spot turn modes according to different power distribution and angle of leg rotation. A dual-mode hybrid controller is designed based on the oblique and 4WS modes, in which multipoint prescanning trajectory tracking control is used for the oblique mode, and incremental linear time-varying model predictive control (ILTV-MPC) is used for the 4WS mode. The constraints required for the dual-mode controller are obtained by experimenting with the test prototype's transverse and longitudinal tracking performance. A joint MATLAB/CARSIM simulation platform is used to compare and verify the performance of each mode controller under two operating conditions. In the first condition, the tracking accuracy of the 4WS mode can be achieved by using the oblique motion mode, and the transverse sway angle variation is significantly reduced. In the second working condition, the oblique motion mode is better than the tracking effect of the 4WS mode overall. The results show that the oblique motion mode can be used instead of the 4WS mode for trajectory tracking under a small-curvature reference trajectory.

1. Introduction

Since the 21st century, more and more attention has been paid to the development of robotics at the national and world level [1]. As an important branch in the field of robotics, mobile robots can replace humans in complex environments for exploration and operation. Therefore, mobile robots have broad application prospects [2]. Wheeled mobility is similar to vehicle mobility with simple structure, high speed, and high-speed maneuverability [3]. Traditional wheeled mobile robots mostly use mecanum wheels as drive wheels, combined with distributed drive methods to achieve all-around mobility, and are widely used in excellent environments such as indoors [4]. However, McNamee wheels have more structure compared to ordinary wheels and are less wear-resistant in complex environments such as

outdoors. Some of the solutions with the Ackermann steering mechanism have poor omnidirectional maneuverability and cannot pass through narrow areas below their steering radius; some of the solutions with distributed drive and differential steering have disadvantages such as high tire wear, low accuracy of calculated position, and difficulty of control [5]. In order to improve the motion control performance of wheeled omnidirectional mobile robots, it is particularly important to propose a scheme with high mobility and high controllability.

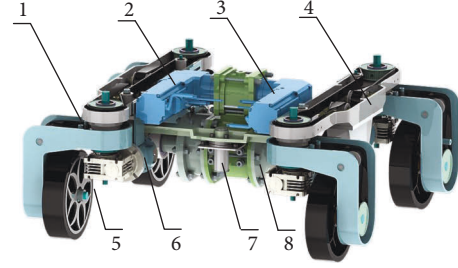
In recent years, the development of the automatic steering controller has attracted more attention [6]. In [7], an adaptive neuron PID controller for nonlinear systems is experimentally verified, but its control parameters need to be determined by extensive engineering tests and are sensitive to vehicle speed. In [8], a side control algorithm for driverless vehicles is based on

the combination of a genetic algorithm and PID. PID, as a feedback link, ensures the accuracy of control. Compared with a PID controller acting alone, it can improve the dynamics characteristics of the system. In [9], a new control method is constructed, the optimal pretargeting driver model lateral position deviation. The number of applications of fuzzy logic in automatic steering control of unmanned vehicles has increased significantly in recent years due to its inherent ability to handle uncertain information and to simulate human logical reasoning and decision making [10]. In [11, 12], the fuzzy controller works well for controlled systems without the complete mathematical model, but coarse parameters of affiliation functions and rule bases tuned by expert experience usually produce overshooting and steady-state errors. In [13], the closed-loop system is represented in the form of linear variables and the Lyapunov controller parameters are tuned by optimally solving the LQR-LMI problem. Model predictive control determines the control input by solving the constrained optimization problem on a rolling basis and has the advantages of a “feed-forward-feedback” control structure, which can also handle the constraints imposed by the kinematic and environmental characteristics of the mobile robot. Model predictive control is widely used in the field of mobile robot trajectory tracking [14]. In [15], model predictive control is used to track the reference trajectory quickly and stably and to ensure the real-time performance of the controller.

To design a mobile robot with all-wheel steering for outdoor complex road conditions. This robot can realize three motion modes. Among them, the multipoint pre-scanning fuzzy compensated lateral tracking controller is used for the oblique motion mode, and the ILTV-MPC controller is used for the 4WS mode. The performance and parameter determination experiments were conducted on the test prototype, and the performance parameters of the prototype obtained from the experiments were used as the constraints of the control system. The designed controller is jointly simulated in MATLAB/CARSIM platform to compare and verify the low-curvature trajectory tracking effect under two motion modes.

2. Mobile Robot Chassis Motion Mode

The structure of the mobile robot chassis is shown in Figure 1. The main motor provides direct power and the auxiliary motor provides differential power. The main and secondary motors providing power are arranged symmetrically. The dual power differential system consists of a differential and electromagnetic clutch, which distributes the speed of the left and right axles through the distribution of the two power flows. The swing-arm travel mechanism with the balance rocker consists of the balance rocker, swing leg, steering motor, and wheels. The swing-arm travel mechanism acts as the actuating part of the power output. The four pendulum legs of the mobile robot chassis rotate independently of each other and the dual power flow system can provide any speed difference between the left and right half-axes within the motor speed range so that a variety of driving modes can be achieved through the combination of different power distribution and steering modes.



1. Swing leg 2. Main motor 3. Sub motor 4. Swing arm
5. Wheel 6. Steering motor 7. Balance rocker arm
8. Dual power differential system

FIGURE 1: Structure of the mobile robot chassis.

2.1. Spot Turn Mode. The spot turn mode allows the mobile robot to pass through narrow areas where steering is not possible. In this mode, the chassis is rotated clockwise or anti-clockwise with the geometric center M as the origin and the extension lines of the four swing leg positions cross the geometric center of the vehicle, as shown in Figure 2.

In order to realize the spot turn function, the main motor holding brake is closed and the auxiliary motor provides differential steering power. In the spot turn mode, the relationship between the swing leg angles is as follows:

$$\begin{aligned} \beta_1 &= \beta_2 \\ &= \beta_3 \\ &= \beta_4 \\ &= \tan^{-1}\left(\frac{L}{H}\right). \end{aligned} \quad (1)$$

2.2. Oblique Motion Mode. The relationship of the swing legs corresponding to the oblique motion mode is shown in Figure 3, which realizes the point-to-point motion, and the yaw angle of the mobile robot chassis does not change during the motion. The relationship between the swing leg angles is as follows:

$$\begin{aligned} \beta_1 &= \beta_2 \\ &= \beta_3 \\ &= \beta_4. \end{aligned} \quad (2)$$

In the oblique motion mode, only the main motor works normally and the electromagnetic clutch is disengaged, which can synchronize. Under the constraint of maximum angle, the oblique steering mode can improve the lateral stability of the mobile robot chassis. Taking advantage of the oblique steering mode, the change of yaw angle during the trajectory tracking can be suppressed to the maximum extent.

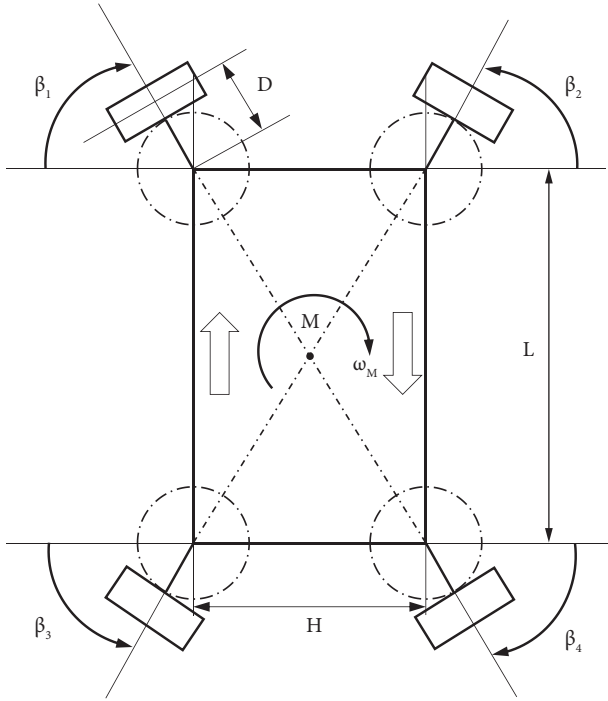


FIGURE 2: Spot turn modes.

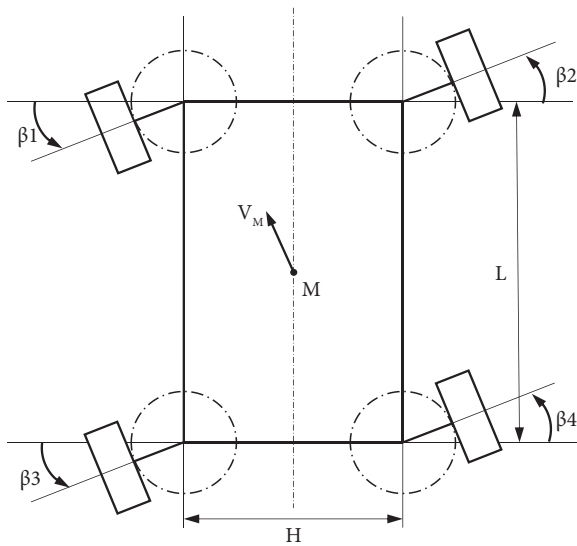


FIGURE 3: Oblique motion modes.

2.3. *4WS Mode.* In the 4WS mode, the relationship between the four swing legs of the mobile robot chassis is shown in Figure 4.

With the same steering angle, the 4WS mode achieves a smaller steering radius compared to the conventional Ackermann steering. Based on the geometric relationship between the pendulum legs, the 4WS mode inner and outer turning angles are related to the turning angle of the virtual wheel on the extension of the center of mass as follows:

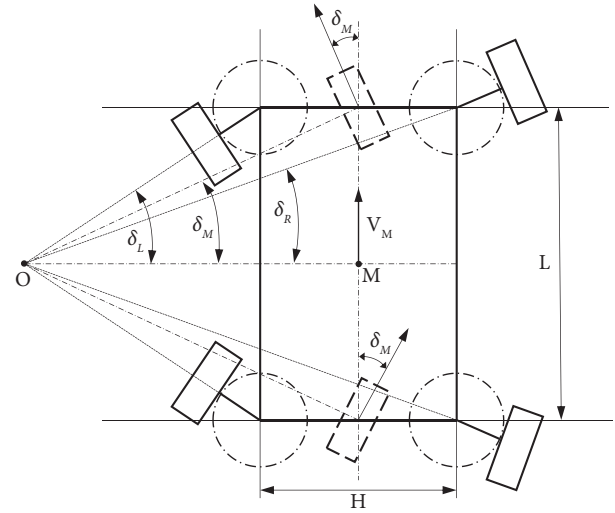


FIGURE 4: 4WS modes.

$$\begin{cases} \frac{L}{\tan \delta_L} + H = \frac{L}{\tan \delta_m}, \\ \frac{L}{\tan \delta_R} - H = \frac{L}{\tan \delta_m}, \\ \frac{0.5L}{\tan \delta_L} + H = \frac{0.5L}{\tan \delta_R}, \end{cases} \quad (3)$$

where L is the swing leg longitudinal distance; H is the swing leg transverse distance; δ_R is the right swing leg turning angle; δ_L is the left swing leg turning angle; and δ_m is the virtual swing leg turning angle.

Neglecting the slip, the relationship between the left and right wheel turning angle and the virtual wheel turning angle on the extension line of the center of mass is derived from the above equation, and the swing leg angle relationship is shown in Figure 5.

3. Dual-Mode Tracking Controllers

3.1. *Multipoint Prescanning Track Fuzzy Compensated Trace Tracking Controller Based on Oblique Motion Modes.* In the low-speed oblique motion mode, all swing legs of the mobile robot chassis turn at the same angle, and their center-of-mass velocity direction is the same as the swing leg rotation direction. Establish the model in Figure 6. The forward prescanning distances of the mobile robot chassis are x_1, x_2, x_3 . The distance between the chassis prescanning point and the track is $d_1, d_2,$ and d_3 , and they are tangent to the track.

The lateral offset from each prescanning point to the direction of the mobile robot chassis is as follows:

$$E_n = \frac{d_n}{\cos(\arcsin(d_n/x_n))}. \quad (4)$$

The prescanning deviation for a series of different prescanning distances on the path can be obtained, and then the

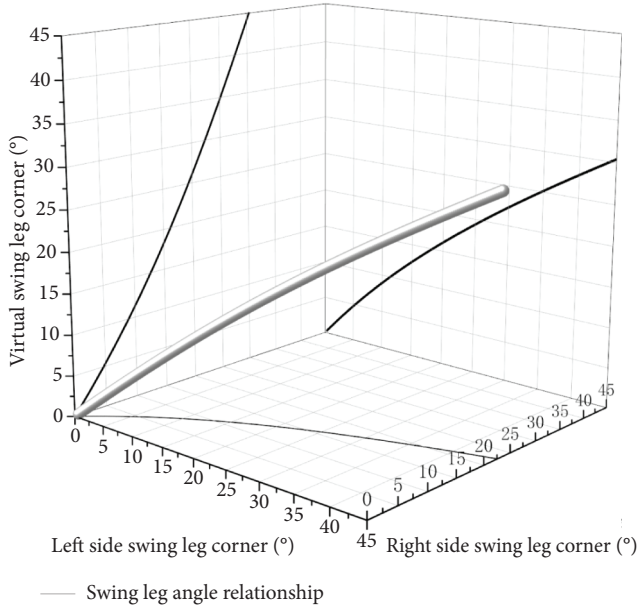


FIGURE 5: Swing leg angle relationship.

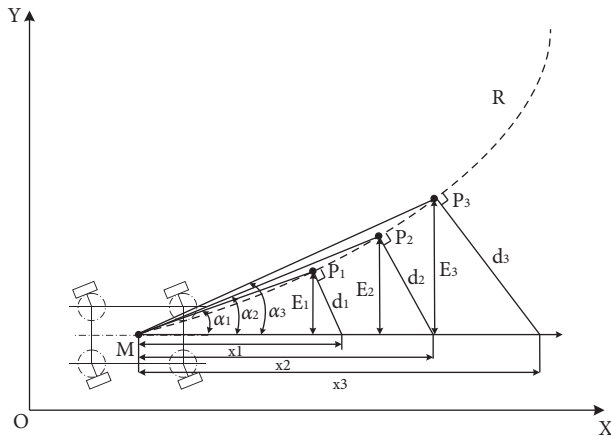


FIGURE 6: Multipoint prescanning model.

offset angle under each prescanning point of the mobile robot chassis is as follows:

$$\alpha_n = \arctan\left(\frac{E_n}{x_n}\right). \quad (5)$$

Then, the swing leg angle control input δ_c at the current control instant is

$$\delta_c = (w_1\alpha_1 + w_2\alpha_2 + w_3\alpha_3), \quad (6)$$

where $w_1, w_2,$ and w_3 are the weight coefficients, and the corresponding weight coefficients for different conditions are shown in Table 1.

3.2. Fuzzy Compensation Control Principle. Due to the use of multiweight multipoint pretargeting, the increased weight of the distal pretargeting point will cause the chassis to turn

TABLE 1: Weighting coefficient assignment.

Conditions	w_1	w_2	w_3
$E_3 \leq 2E_2$	0.3	0.2	0.5
$E_3 \geq 2E_2$	0.7	0.2	0.1
$E_3 \leq 2E_2$ and $E_2 \leq 2E_1$	0.1	0.2	0.7

early, thus causing the chassis steering error. To achieve a more accurate trajectory tracking effect, the chassis turning angle is compensated by using fuzzy control. The weighted pretargeting point lateral deviation E_m and dE_m/dt obtained when the distal pretargeting point weight is 0.7 are selected as the input of the two-dimensional fuzzy system, and b is the fuzzy system output.

The input-output fuzzy set of the system is defined as follows:

$$\begin{aligned} E_m &= \{NB, NS, NL, PL, PS, PB\}, \\ \dot{E}_m &= \{NB, NS, ZO, PS, PB\}, \\ b &= \{NB, NS, NL, ZO, PL, PS, PB\}, \end{aligned} \quad (7)$$

where the E_m domain is $[-0.85, 0.85]$, the dE_m/dt domain is $[-1, 1]$, and b is the fuzzy system output. NB is “negative large,” NS is “negative medium,” NL is “negative small,” ZO is “zero,” PL is “positive small,” PS is “positive medium,” and PB is “positive large.”

After getting the fuzzy set, fuzzy rules are established for the input and output, and the fuzzy rule table can be obtained as shown in Table 2.

The fuzzy controller is designed in MATLAB, and the output fuzzy system control surface is obtained as shown in Figure 7.

The output b is obtained by using the “area center of gravity method” for defuzzification.

$$b = \frac{\sum_{i=1}^n b_i \mu_c(b_i)}{\sum_{i=1}^n \mu_c(b_i)}. \quad (8)$$

The combination of (6) and (8) yields a swing leg control angle of δ_f as

$$\delta_f = \delta_c + b. \quad (9)$$

3.3. ILTV-MPC Trajectory Tracking Controller Based on 4WS Mode. A two-degree-of-freedom vehicle kinematic model is used for analysis, and to simplify the calculation, it is assumed that the mobile robot chassis does linear motion or circular motion around a point at any moment and ignores the role of the suspension. The vehicle inertial coordinate system XOY is shown in Figure 8, and the X-axis is defined to point due east and the Y-axis is defined to point due north.

The velocity at the geometric center m of the mobile robot chassis is

$$V_m = \dot{X}_m \cos \varphi + \dot{Y}_m \sin \varphi. \quad (10)$$

The kinematic constraints and geometric relations between front axis and the geometric center are

TABLE 2: Fuzzy rules.

E_m	NB	NS	NL	PL	PS	PB	PB	NB	PB
dE_m/dt	ZO	ZO	ZO	ZO	ZO	ZO	ZO	NB	PB
b	NB	NS	NL	ZO	PL	PS	PB	NB	PB

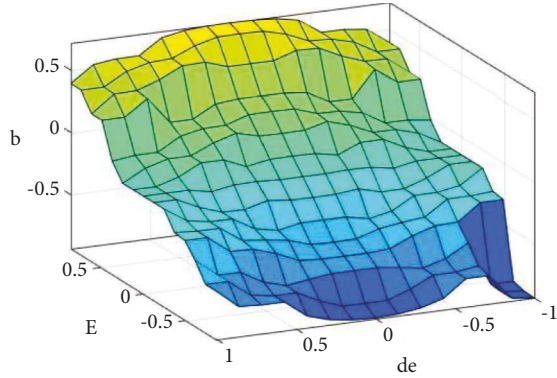


FIGURE 7: System control surface.

$$\begin{aligned}
 \dot{X}_f \sin(\varphi + \delta_m) - \dot{Y}_f \cos(\varphi + \delta_m) &= 0, \\
 \dot{X}_m \sin \varphi - \dot{Y}_m \cos \varphi &= 0, \\
 X_f &= X_m + 0.5L \cos \varphi, \\
 Y_f &= Y_m + 0.5L \sin \varphi.
 \end{aligned} \tag{11}$$

From (10) and (11), the kinematic equation of the mobile robot chassis is obtained as

$$\begin{bmatrix} \dot{X}_m \\ \dot{Y}_m \\ \dot{\varphi} \end{bmatrix} = \begin{bmatrix} \cos \varphi \\ \sin \varphi \\ \frac{2 \tan \delta_m}{L} \end{bmatrix} V_m, \tag{12}$$

where (X_m, Y_m) represents the geometric center coordinates of the mobile robot chassis; φ is the transverse swing angle of the mobile robot chassis; δ_m is the front and rear wheel deflection angle; V_m is the geometric center velocity; and L is the axis distance.

From (12), the system consists of state $\dot{\chi} = [\dot{X}_m \ \dot{Y}_m \ \dot{\varphi}]^T$ with input $u = [V_m \ \delta_m]^T$. Its general form is

$$\dot{\chi} = f(\chi, u). \tag{13}$$

For a known reference trajectory, which can be represented by the trajectory of the reference vehicle, the points on the reference trajectory all satisfy the kinematic equations, and the general form of the reference r is

$$\dot{\chi}_r = f(\chi_r, u_r), \tag{14}$$

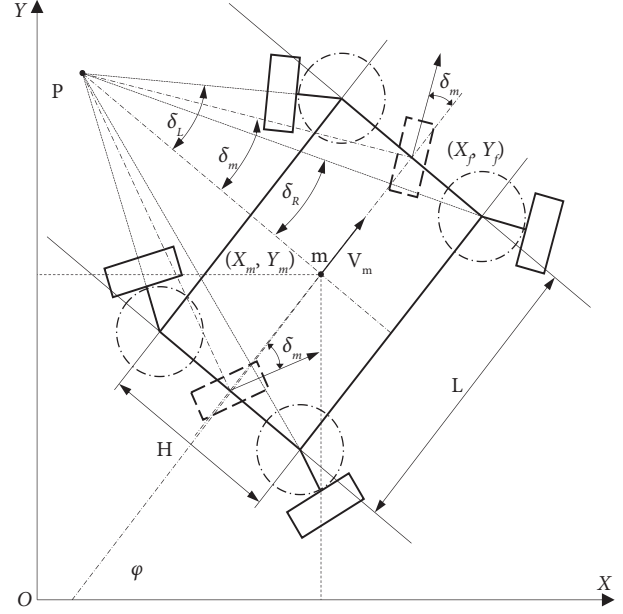


FIGURE 8: 4WS kinematic model.

where $\dot{\chi}_r = [\dot{X}_r \ \dot{Y}_r \ \dot{\varphi}_r]^T$ and $u_r = [V_m \ \delta_m]^T$.

Equation (13) is subtracted from equation (14) at the reference trajectory using a Taylor series expansion and neglecting the higher order terms. The resulting linear error model of the mobile robot chassis is discretized to obtain

$$\tilde{\chi}(k+1) = A_{k,t} \tilde{\chi}(k) + B_{k,t} \tilde{u}(k), \tag{15}$$

where $A_{k,t} = \begin{bmatrix} 1 & 0 & -V_r \sin \varphi_r T \\ 0 & 1 & V_r \cos \varphi_r T \\ 0 & 0 & 1 \end{bmatrix}$; $B_{k,t} = \begin{bmatrix} \cos \varphi_r T & 0 \\ \sin \varphi_r T & 0 \\ 2 \tan \delta_r T/L & 2V_r T/L \cos^2 \delta_r \end{bmatrix}$; and T is the sampling time.

Transforming the control inputs into increments, the state space expression for an incremental linear time-varying system combining the output is

$$\begin{aligned}
 \xi(k+1|t) &= \tilde{A}_{k,t} \xi(k|t) + \tilde{B}_{k,t} \Delta U(k|t), \\
 \eta(k|t) &= \tilde{C}_{k,t} \xi(k|t),
 \end{aligned} \tag{16}$$

where $\tilde{A}_{k,t} = \begin{bmatrix} A_{k,t} & B_{k,t} \\ 0_{m \times n} & I_m \end{bmatrix}$; $\tilde{B}_{k,t} = \begin{bmatrix} B_{k,t} \\ I_m \end{bmatrix}$; n is the state volume dimension; and m is the control volume dimension.

To ensure the real-time nature of the controller, approximation of $A_{k,t}$ and $B_{k,t}$ is handled as follows:

$$\begin{aligned}
 A_{k,t} &= A_{t,t}, \quad k = 1, 2, \dots, t + N - 1, \\
 B_{k,t} &= B_{t,t}, \quad k = 1, 2, \dots, t + N - 1.
 \end{aligned} \tag{17}$$

3.4. Constraint Conditions and Optimal Solution. The situation that the optimal solution is not available in the predicted time domain can occur during the real-time change of the system model. Thus, a relaxation factor is introduced to make a feasible solution for each optimization. In designing the trajectory tracking controller, the objective function optimized in the literature [10] takes the following form:

$$J(k) = \sum_{i=1}^{N_p} \eta(k+i|t) - \eta_{\text{ref}}(k+i|t)_Q^2 + \sum_{i=1}^{N_c-1} \Delta U(k+i|t)_R^2 + \rho \varepsilon^2, \quad (18)$$

where N_p denotes the prediction time domain; N_c denotes the control time domain; ρ denotes the weight coefficient; ε denotes the relaxation factor; Q denotes the weight matrix of output deviations; and R denotes the weight matrix of control increments.

To ensure that the all-wheel steering mobile robot chassis is fast and stable for trajectory tracking, optimization of the system control volume needs to be incorporated; constraints on the control inputs are expressed in the form of

$$u_{\min}(t+k) \leq u(t+k) \leq u_{\max}(t+k), \quad (19)$$

$$k = 0, 1, 2, \dots, N_c - 1.$$

The constraint on control increment is expressed in the following form:

$$u_{\min}(t+k) \leq \Delta u(t+k) \leq \Delta u_{\max}(t+k), \quad (20)$$

$$k = 0, 1, 2, \dots, N_c - 1.$$

The above equation is converted into the form of control increment or control increment multiplied with the transformation matrix, and finally, the objective function combined with the constraints is transformed into the standard quadratic form for the computer solution as follows:

$$J(\xi(t), u(t-1), \Delta U_t) = \begin{bmatrix} \Delta U(t)^T \\ \varepsilon \end{bmatrix}^T H_t \begin{bmatrix} \Delta U(t)^T \\ \varepsilon \end{bmatrix} + G_t \begin{bmatrix} \Delta U(t)^T \\ \varepsilon \end{bmatrix} \quad (21)$$

$$\text{s.t.} \begin{cases} U_{\min} \leq A * \Delta U_t + \Delta U_t \leq U_{\max}, \\ \Delta U_{\min} \leq \Delta U_t \leq \Delta U_{\max}, \\ \varepsilon > 0. \end{cases}$$

3.5. Feedback Correction. In one control cycle, a series of control input increments in the control time domain is obtained upon obtaining the solution of (21):

$$\Delta U_t^* = [\Delta u_t^*, \Delta u_{t+1}^*, \dots, \Delta u_{t+N_c-1}^*]^T. \quad (22)$$

Taking the first element of this series of control input increments as the control input increment of the actual system, the input to the system at this moment is

$$u(t) = u(t-1) + \Delta u_t^*. \quad (23)$$

The system executes this control input until the next control cycle, uses the new state information to repredict the sequence of control input increments for the next control time domain, and then applies its first element to the system to execute the next control cycle. In this way, the incremental linear time-varying model predictive trajectory tracking control of the mobile robot chassis is achieved.

4. Experiments and Simulations

4.1. Vehicle Parameters and Constraint Determination Experiments. The structural parameters of the mobile robot chassis are total chassis length (810 mm), total width (720 mm), total height (360 mm), total mass (65 kg), swing leg length ($D=90$ mm), horizontal distance ($H=396$ mm), vertical distance ($L=500$ mm), wheel radius ($r=90$ mm), main and secondary motor power (0.4 KW), and torque (1.27 N·m). The lateral and longitudinal tracking experiments were conducted on a good asphalt road, as shown in Figure 9. Among them, Figure 9(a) shows the swing leg limit angle of the prototype in 4WS modes, Figure 9(b) shows the

swing leg limit angle of the prototype in oblique motion modes, and Figure 9(c) shows the swing leg limit angle of the prototype in spot turn modes.

The lateral tracking ability experiment of chassis test prototype of mobile robot can get the angle constraint and angle increment constraint of controller. In the tracking ability experiment of three operating modes, the limit angle and limit angle rotation time of the swing leg were recorded, and the test results are shown in Table 3.

Then, the turning angle δ_m and the increment of turning angle $\Delta\delta_m$ in 4WS mode are

$$\begin{aligned} -16.12^\circ &\leq \delta_m \leq 16.12^\circ, \\ -2.093^\circ &\leq \Delta\delta_m \leq 2.093^\circ. \end{aligned} \quad (24)$$

In the longitudinal tracking capability experiment, the desired speed of the robot was set to 1 and 2, and the acceleration and deceleration times, as shown in Table 4, were obtained by decelerating with the maximum braking force 5 seconds after reaching the desired speed.

From the experimental data, it can be obtained that the acceleration process of the mobile robot chassis is smooth and the acceleration is kept at around 0.41 m/s^2 . Combining with the acceleration characteristics of the mobile robot chassis, the velocity constraint can be set as follows:

$$\begin{aligned} -0.3 &\leq v - v_d \leq 0.3, \\ -0.06 &\leq \Delta v \leq 0.06, \end{aligned} \quad (25)$$

where v_d is the desired vehicle speed and Δv is the speed increment per control cycle.

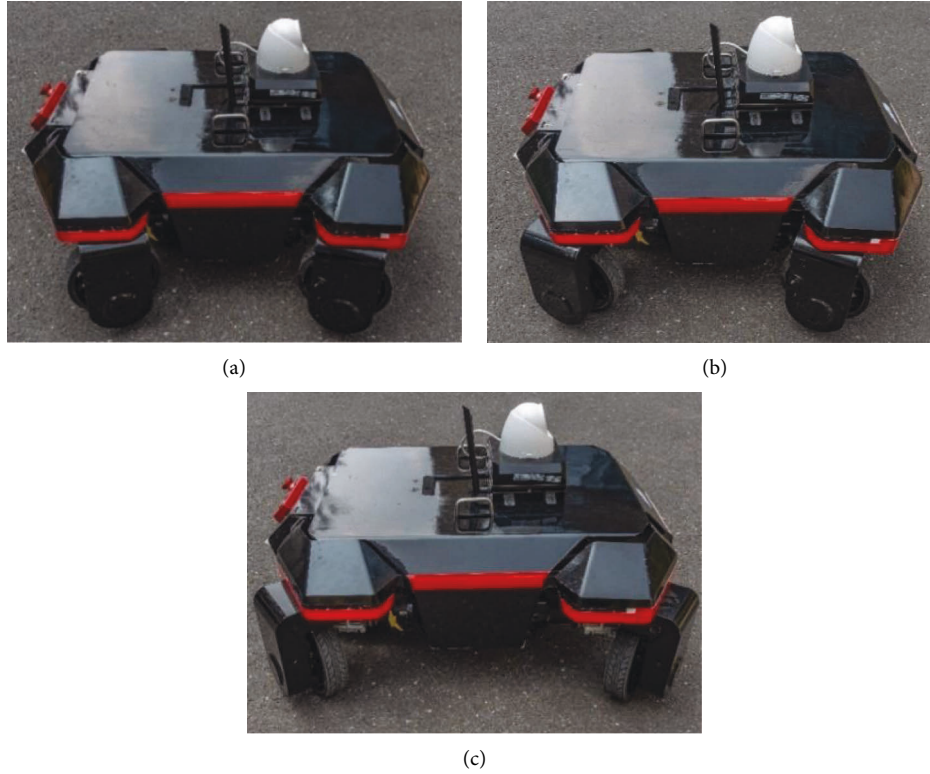


FIGURE 9: Test prototype. (a) 4WS mode. (b) Oblique motion mode. (c) Spot turn mode.

TABLE 3: Lateral tracking capability.

Operation modes	Internal and external swing leg angle $\delta/^\circ$	Time spent in leg swing t/s
4WS modes	19.96	0.682
	13.78	0.476
Oblique motion modes	14.92	0.507
	14.96	0.510
Spot turn modes	56.84	1.942
	56.88	1.949

TABLE 4: Lateral tracking capability.

Test speed interval	Acceleration time t/s	Brake time t/s
0~1 m/s	2.2	2.3
0~2 m/s	3.4	3.6

4.2. Comparative Simulation of Dual-Mode Trajectory Tracking. To investigate the performance of the proposed framework presented in Section 2, numerical simulations with the controller have been conducted using vehicle simulation software, CARSIM, and MATLAB/SIMULINK. Figure 10 shows the block diagram of the implementation, and the driving modes are selected by manual switching and automatic switching. In the automatic switching mode, the driving mode judgment receives the δ_f output of the multipoint prescan controller with the δ_m and V_m of the MPC controller. If δ_m is greater than 5° , 4WS mode will be selected for trajectory tracking; if δ_m is less than 5° , oblique motion mode will be selected for trajectory tracking. The mode selected will be

carried on until the next control cycle for mode transition.

Import the mobile robot chassis structure parameters into the CARSIM model and set the road adhesion coefficient to 0.85 and the reference speed to 1 m/s. The reference trajectory of working condition one is shown in Figure 11, and the expression of the reference trajectory is

$$y = -(\sin(0.1x\pi + 0.5\pi) - 1). \quad (26)$$

To test the small-curvature trajectory tracking capability of the mobile robot chassis, trajectory tracking simulations were performed on the chassis in the desired trajectory using oblique motion mode and 4WS mode, respectively, and the tracking performance of different modes was compared and verified.

The lateral position error is shown in Figure 12(a), the maximum error of the lateral position of the oblique motion mode controller is 6.77 cm, the average error is 2.48 cm, and the root mean square error is 3.21%. The maximum error of the lateral position of the 4WS mode controller is 4.05 cm,

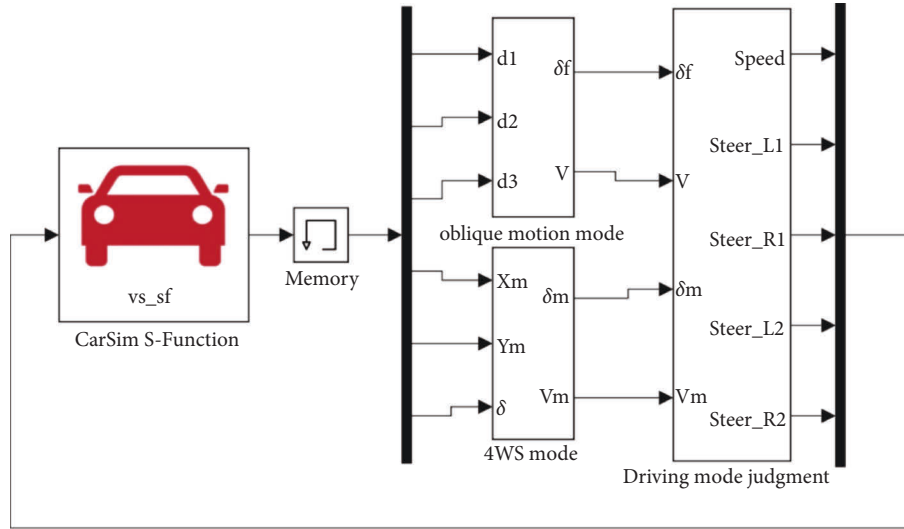


FIGURE 10: Control strategy block diagram.

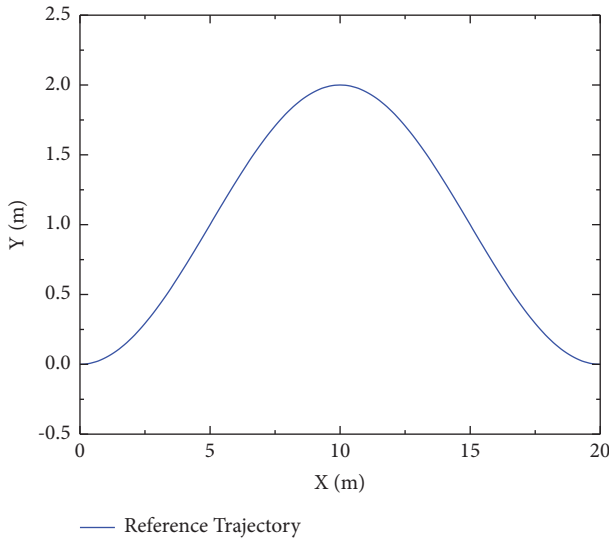


FIGURE 11: Reference trajectory.

the average error is 2.44 cm, and the root mean square error is 2.72%. The longitudinal position error is shown in Figure 12(b), the maximum error of the longitudinal position of the oblique motion mode controller is 8.02 cm, the average error is 4.33 cm, and the root mean square error is 4.91%. The maximum error of the longitudinal position of the 4WS mode controller is 9.27 cm, the average error is 3.57 cm, and the root mean square error is 4.30%. The oblique motion mode used by the hybrid controller on small-curvature path can achieve the tracking effect of the 4WS mode. Analysis of Figure 12(c) shows that the swing leg angle in the 4WS mode changes in a small range with time and within $\pm 4.1^\circ$. The steering motor in the 4WS mode needs to adjust the swing leg angle all the time, which causes the error of the steering swing leg angle. Figure 12(d) shows that the swing leg angle remains stable when increasing to 13.3° in the diagonal travel mode. The dynamic adjustment of the

steering motor is reduced, which leads to the improvement of the trajectory tracking accuracy on small-curvature path. 4WS mode and diagonal travel mode in tracking the first part of the reference trajectory with the change of the transverse swing angle are shown in Figure 12(e). The transverse sway angle of the chassis remains unchanged, and the transverse sway angle varies within $\pm 18.7^\circ$ in the 4WS mode. The mobile robot chassis can significantly reduce the transverse sway angle variation by using the oblique motion mode and make the angle equal to that in another mode. Compared with the 4WS mode, the advantage of small swing angle variation in the oblique motion mode enables the mobile robot chassis to achieve small-curvature trajectory tracking and improve its transverse stability.

The reference trajectory of working condition 2 is piecewise, the first and third parts are five-meter straight lines, and the second part is a ramp with a slope of 0.2 for changing lanes, and the reference trajectory is shown in Figure 13.

Condition 2 focuses on testing the stability of each controller of the mobile robot chassis when the curvature of the reference trajectory varies discontinuously. The tracking performance of the chassis under different modes is compared and analyzed.

The lateral position error is shown in Figure 14(a), the maximum error of the lateral position of the ramp mode controller is 3.41 cm, the average error is 1.07 cm, and the root mean square error is 1.49%. The maximum error of the lateral position of the 4WS mode controller is 6.05 cm, the average error is 1.88 cm, and the root mean square error is 3.08%. The maximum lateral error occurred in the 10 m to 20 m section, but the oblique motion mode could transition to the desired state more quickly. The longitudinal position error is shown in Figure 14(b), the maximum error of the longitudinal position of the ramp mode controller is 7.08 cm, the average error is 2.30 cm, and the root mean square error is 3.22%. The maximum error of the longitudinal position of the 4WS mode controller is 6.20 cm, the average error is

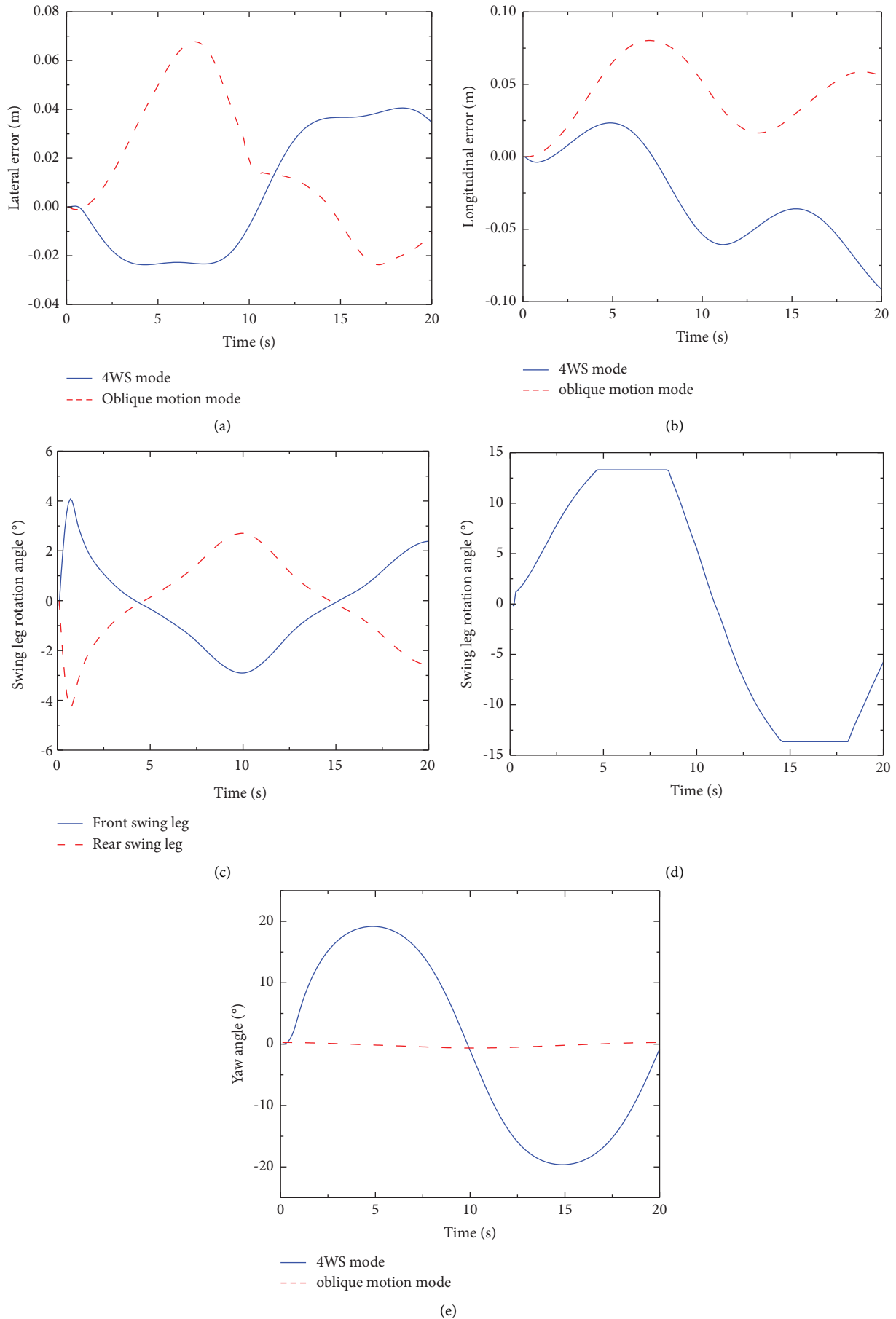


FIGURE 12: Response results of system states in condition 1 simulation test. (a) Lateral error. (b) Longitudinal error. (c) 4WS mode. (d) Oblique motion mode. (e) Yaw angle of different modes.

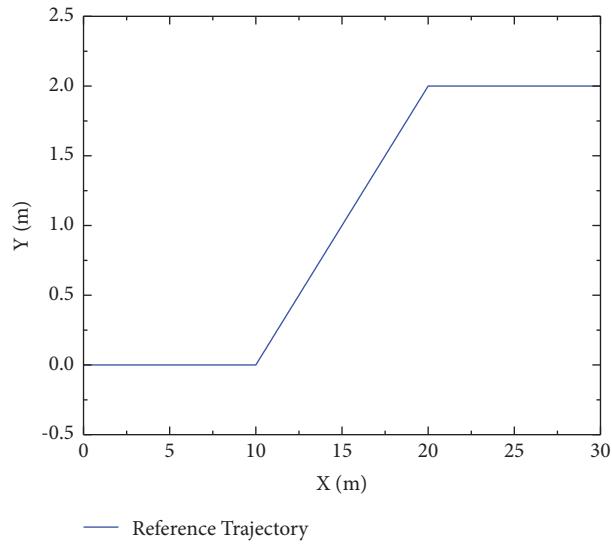
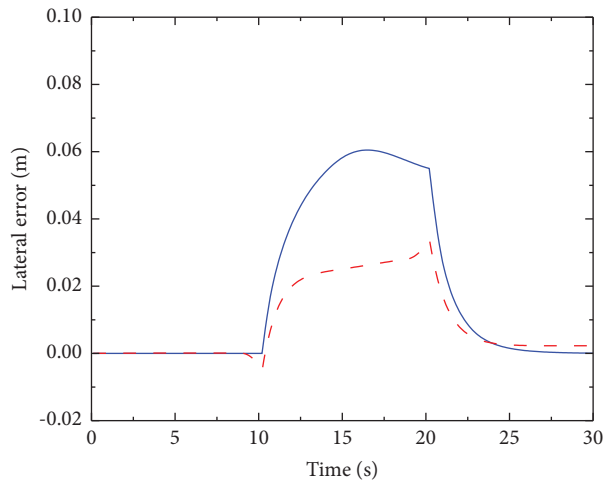
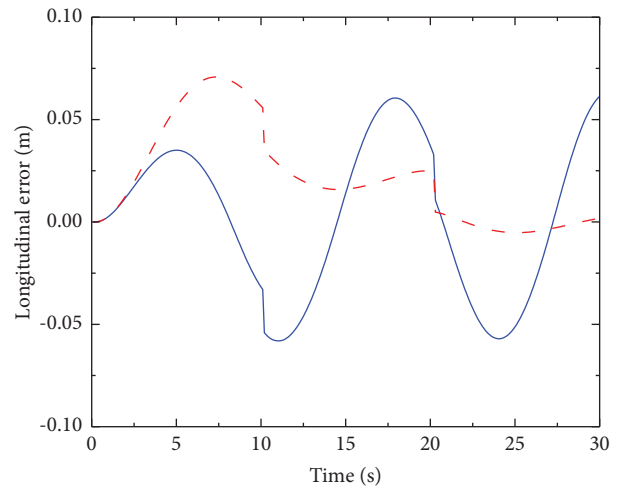


FIGURE 13: Reference trajectory.



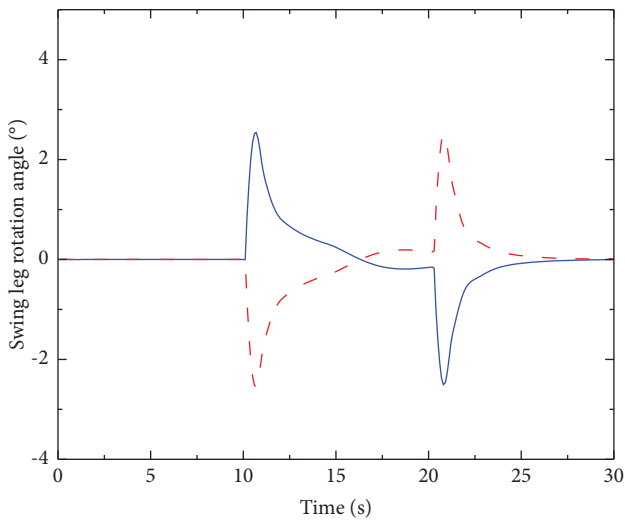
— 4WS mode
 - - - Oblique motion mode

(a)



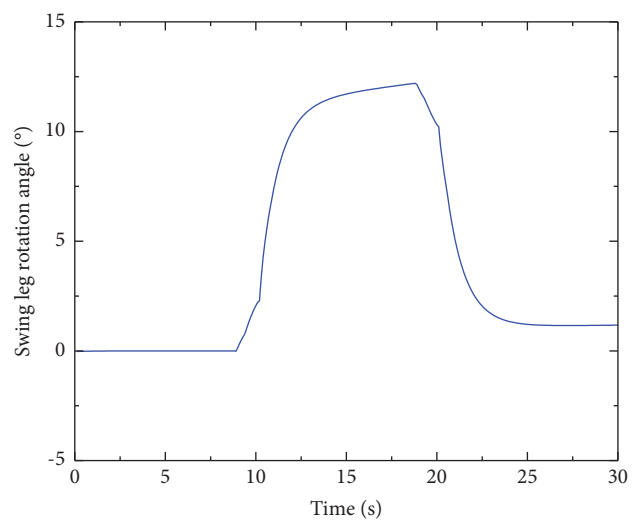
— 4WS mode
 - - - oblique motion mode

(b)



— Front swing leg
 - - - Rear swing leg

(c)



(d)

FIGURE 14: Continued.

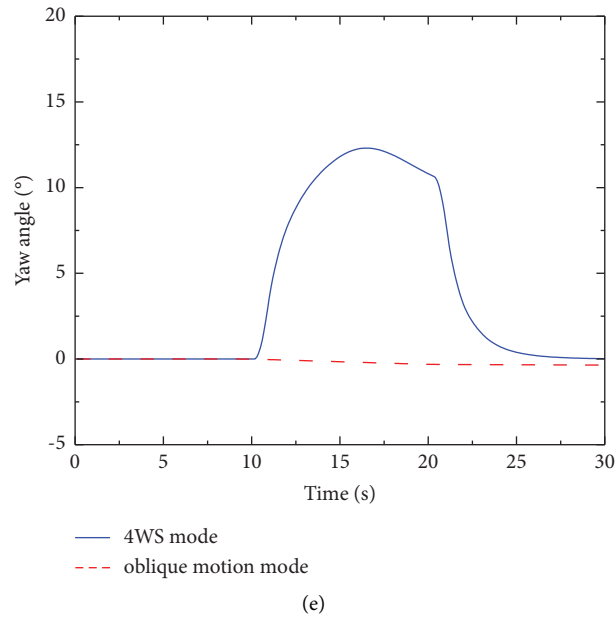


FIGURE 14: Response results of system states in condition 2 simulation test. (a) Lateral error. (b) Longitudinal error. (c) 4WS mode. (d) Oblique motion mode. (e) Yaw angle of different modes.

3.24 cm, and the root mean square error is 3.74%. The oblique motion mode ensures that the longitudinal error converges to zero when the curvature of the reference trajectory varies discontinuously. Figure 14(c) shows that the swing leg turning angle in the 4WS mode changes within $\pm 2.54^\circ$ in a small time range. During the real vehicle test, the steering motor in 4WS mode needs to adjust the swing leg at a small angle at all times, which causes the error of the steering swing leg angle. Figure 14(d) shows that the maximum swing leg angle of 12.2° is achieved in the oblique motion mode. In the 10 m and 20 m sections, the angle range is controlled within 1.23° . Yaw angles of the robot in the two modes are shown in Figure 14(e). The chassis transverse sway angle is maintained, and the transverse sway angle varies within $\pm 18.7^\circ$ in the 4WS mode. The angle can be significantly reduced using the oblique motion mode. Compared with the 4WS mode, the oblique motion mode has the advantage of small swing angle variation, which enables the mobile robot chassis to achieve small-curvature trajectory tracking and improve its transverse stability.

5. Conclusion

- (1) A mobile robot chassis structure with a dual power differential power system and a common wheel as the driving wheel is proposed. The kinematic model of each steering mode of the mobile robot chassis is established, the corresponding principles are analyzed to derive its motion control strategy, and the correctness of the design is verified theoretically. The prototype was tested in lateral and longitudinal tracking to verify the theoretical feasibility of the designed mobile robot chassis and to determine the required constraints of each controller.

- (2) When the mobile robot chassis is performing small-curvature trajectory tracking, the oblique motion mode can achieve the trajectory tracking effect of the 4WS mode. The swing leg angle is more stable than the 4WS mode when the curvature of the small-curvature reference trajectory suddenly changes, which improves the control accuracy of the swing leg, and the transverse swing angle of the mobile robot chassis maintains the initial value of the oblique motion mode. The oblique motion mode improves the trajectory tracking stability of the all-wheel steering robot under small curvature while achieving trajectory tracking accuracy.

Data Availability

Publicly archived datasets analyzed or generated during the study are available upon request from the authors.

Conflicts of Interest

The authors declare that they have no conflicts of interest.

Acknowledgments

This study was funded by the Open Research Fund Program of Beijing Engineering Research Center of Monitoring for Construction Safety (BJC2020K007).

References

- [1] N. Ding, C. Peng, M. Lin, and C. Wu, "A comprehensive review on automatic mobile robots: applications, perception, communication and control," *Journal of Circuits, Systems, and Computers*, vol. 31, p. 08, 2022.

- [2] X. Li, Z. Sun, D. Cao, D. Liu, and H. He, "Development of a new integrated local trajectory planning and tracking control framework for autonomous ground vehicles," *Mechanical Systems and Signal Processing*, vol. 87, pp. 118–137, 2017.
- [3] T. Ding, Y. Zhang, G. Ma, Z. Cao, X. Zhao, and B. Tao, "Trajectory tracking of redundantly actuated mobile robot by MPC velocity control under steering strategy constraint," *Mechatronics*, vol. 84, no. 2022, Article ID 102779, 2022.
- [4] X. Li, H. Wolfgang, X. Weiliang, and A. S. Karl, "Experimental validation of energy consumption model for the four-wheeled omnidirectional Mecanum robots for energy-optimal motion control," in *Proceedings of the 2016 IEEE 14th International Workshop on Advanced Motion Control*, (AMC) IEEE, Auckland, New Zealand, June 2016.
- [5] Z. Chen, X. Xie, F. Gao, Z. Liu, and Y. Li, "Pure rolling steering system design and Research for wheeled mobile robot," *Journal of Physics: Conference Series*, vol. 1345, no. 4, Article ID 042071, 2019.
- [6] L. Li, J. Li, and S. Zhang, "Review article: state-of-the-art trajectory tracking of autonomous vehicles," *Mechanical Sciences*, vol. 12, no. 1, pp. 419–432, 2021.
- [7] E. Freire, F. G. Rossomando, and C. M. Soria, "Self-tuning of a neuro-adaptive PID controller for a SCARA robot based on neural network," *IEEE Latin America Transactions*, vol. 16, no. 5, pp. 1364–1374, 2018.
- [8] B. Zhao, H. Wang, L. Qing, L. Jingkai, and Z. Yuefei, "PID trajectory tracking control of autonomous ground vehicle based on genetic algorithm," in *Proceedings of the 2019 Chinese Control And Decision Conference (CCDC) 0*, Nanchang, China, June 2019.
- [9] H. Z. Li, L. Li, J. Song, and L. Y. Yu, "Comprehensive lateral driver model for critical maneuvering conditions," *International Journal of Automotive Technology*, vol. 12, no. 5, pp. 679–686, 2011.
- [10] C. Zhang, J. Hu, J. Qiu, W. Yang, H. Sun, and Q. Chen, "A novel fuzzy observer-based steering control approach for path tracking in autonomous vehicles," *IEEE Transactions on Fuzzy Systems*, vol. 2, p. 1, 2018.
- [11] X. Wang, M. Fu, H. Ma, and Y. Yang, "Lateral control of autonomous vehicles based on fuzzy logic," *Control Engineering Practice*, vol. 34, pp. 1–17, 2015.
- [12] S. Allou and Y. Zennir, "A comparative study of PID-PSO and fuzzy controller for path tracking control of autonomous ground vehicles," in *Proceedings of the 15th International Conference on Informatics in Control, Automation and Robotics*, Mavrovo, Macedonia, April 2018.
- [13] E. Alcalá, V. Puig, J. Quevedo, T. Escobet, and R. Comasolivas, "Autonomous vehicle control using a kinematic Lyapunov-based technique with LQR-LMI tuning," *Control Engineering Practice*, vol. 73, pp. 1–12, 2018.
- [14] J. Liu, P. Jayakumar, J. L. Stein, and T. Ersal, "A nonlinear model predictive control formulation for obstacle avoidance in high-speed autonomous ground vehicles in unstructured environments," *Vehicle System Dynamics*, vol. 56, no. 6, pp. 853–882, 2017.
- [15] J. Liu, P. Jayakumar, J. L. Stein, and T. Ersal, "Improving the robustness of an MPC-based obstacle avoidance algorithm to parametric uncertainty using worst-case scenarios," *Vehicle System Dynamics*, vol. 51, 2019.